Search potential for direct slepton pair production at the CEPC with $\sqrt{s}$ = 360 GeV*

Feng Lyu (吕峰)[1†] Jiarong Yuan (袁家荣)[1,2] Huajie Cheng (程华杰)[3] Jianxiong Wang (王建雄)[1,2]
Rabia Hameed[1,2] Da Xu (徐达)[1,2] Xuai Zhuang (庄胥爱)[1,2,4‡]

[1]Institute of High Energy Physics, Chinese Academy of Sciences, Beijing 100049, China
[2]University of the Chinese Academy of Sciences, Beijing 100049, China
[3]Department of Basic Courses, Naval University of Engineering, Wuhan 430033, China
[4]Institute of Physics, Henan Academy of Sciences, Zhengzhou 450046, China

Abstract: The Circular Electron Positron Collider (CEPC) is designed to operate at key center-of-mass energies: 91.2 GeV as a Z factory for precision Z boson studies, ≈ 160 GeV at the threshold for W boson pair production, and 240 GeV as a Higgs factory for copious Higgs boson production. It can be upgraded to 360 GeV (CEPC-360 GeV) for enabling top quark-antiquark ($t\bar{t}$) pair production. Beyond enabling high-precision measurements of the Standard Model (SM), CEPC-360 GeV is uniquely positioned to perform searches for new physics beyond the SM (BSM), serving as a valuable complement to hadron colliders. This paper presents a sensitivity study on the direct pair production of staus and smuons at the CEPC with $\sqrt{s}$ = 360 GeV, conducted via full Monte Carlo simulation. Under the assumptions of 1.0 ab^{-1} integrated luminosity and a flat 5% systematic uncertainty, CEPC-360 GeV could potentially discover the combined production of left-handed and right-handed staus up to a mass of 170 GeV (if they exist) or up to 169 for pure left-handed staus and 162 GeV for pure right-handed staus. For direct smuon production, the discovery potential reaches up to 178 GeV under the same conditions.

Keywords: CEPC, SUSY, slepton, new physics

DOI: 10.1088/1674-1137/ae2f4e **CSTR:** 32044.14.ChinesePhysicsC.50033001

I. INTRODUCTION

Supersymmetry (SUSY) [1−7] postulates the existence of a supersymmetric partner for each Standard Model (SM) particle, with the spin of the partner differing by one-half unit. In models conserving R-parity [8], SUSY particles are produced in pairs. Following a chain of decays, the lightest supersymmetric particle (LSP) remains stable and emerges as a compelling candidate for dark matter [9, 10].

In simplified SUSY models involving only electroweak interactions, the SUSY particle spectrum comprises charginos ($\tilde{\chi}_i^{\pm}$, where $i = 1,2$ and ordered by increasing mass), neutralinos ($\tilde{\chi}_i^0$, $i = 1,2,3,4$), charged sleptons ($\tilde{l}$), and sneutrinos ($\tilde{\nu}$). Charginos and neutralinos are mass eigenstates formed by linear combinations of the superpartners of Higgs bosons and electroweak gauge bosons. Sleptons, the superpartners of charged leptons, are categorized as left-handed ($\tilde{l}_L$) or right-handed ($\tilde{l}_R$) based on the chiralities of their SM counterparts. The mass eigenstates of sleptons, denoted as $\tilde{l}_i$ ($i = 1,2$ and ordered by increasing mass), arise from mixing $\tilde{l}_L$ and $\tilde{l}_R$. In this study, we assume mass degeneracy between $\tilde{l}_L$ and $\tilde{l}_R$.

Models featuring light staus can produce dark matter relic densities consistent with cosmological observations [11]. Light sleptons also play a role in neutralino co-annihilation processes in the early universe [12, 13]. In both gauge-mediated [14−16] and anomaly-mediated [17, 18] supersymmetry breaking models, slepton masses are expected to be on the order of 100 GeV.

Previous searches for direct slepton pair production have been performed at the Large Electron-Positron Collider (LEP) and the Large Hadron Collider (LHC). At the LEP, stau (smuon) masses below 96 (99) GeV were excluded for mass splittings between the slepton and the

Received 8 January 2025; Accepted 18 December 2025; Accepted manuscript online 19 December 2025
* Supported by the State Key Program of National Natural Science of China (2018YFA0404000, 12135013)
† E-mail: luf@ihep.ac.cn
‡ E-mail: zhuangxa@ihep.ac.cn (Corresponding author)

LSP greater than 7 (4) GeV [19–24]. At the LHC, slepton masses up to 700 GeV were excluded at the 95% confidence level for a massless LSP [25, 26]. However, sensitivity diminishes for compressed mass spectra: for example, slepton masses up to 251 GeV are excluded for a mass splitting of approximately 10 GeV [27]. Using 139 fb^{-1} of ATLAS data, stau masses up to 500 GeV are excluded at the 95% confidence level [28]; with 77.2 fb^{-1} of CMS data, masses between 90 and 120 GeV are excluded under the assumption of a nearly massless LSP [29]. For small mass splittings between the slepton and the LSP, sensitivity remains highly limited at hadron colliders, applying to the LHC [30] and the projected performance of the High Luminosity LHC (HL-LHC) [31], which is not expected to resolve this limitation. Challenges posed by such compressed regions at the LHC and HL-LHC arise from difficulties in reconstructing low-energy leptons and severe background contamination, which are limitations that highlight the unique advantages of lepton colliders.

The Circular Electron Positron Collider (CEPC) [32] is designed to operate at key center-of-mass energies: 91.2 GeV as a Z factory for precision Z boson studies, ≈ 160 GeV at the threshold for W boson pair production, and 240 GeV as a Higgs factory for copious Higgs boson production. This can be upgraded to 360 GeV (CEPC-360 GeV), which is an energy near the $t\bar{t}$ threshold that enhances sensitivity to physics beyond the SM (BSM). A slepton search using CEPC-240 GeV with 5.05 ab^{-1} of integrated luminosity has already been performed: under this configuration, CEPC-240 GeV shows the potential to discover a combined left- and right-handed stau production up to 116 GeV, or up to 113 GeV for pure $\tilde{l}_L$ or $\tilde{l}_R$ scenarios. For smuon production, the discovery potential reaches 117 GeV under the same conditions [33]. This paper presents an analysis of the potential for slepton pair production at CEPC-360 GeV with 1.0 ab^{-1} of integrated luminosity.

Similar to the CEPC, the International Linear Collider (ILC) and Future Circular Collider for electrons and positrons (FCC-ee) are proposed electron-positron colliders [34, 35]. The CEPC and FCC-ee are circular colliders designed to operate at multiple center-of-mass energies ranging from 90 to 360 GeV, while the ILC is a linear collider with planned energies spanning 250 GeV to 1 TeV. Drawing on prior LEP-based studies [36], a conservative systematic uncertainty of 5% is adopted in this analysis. The results presented in this paper are expected to be largely independent of specific detector, trigger, and data acquisition details, which makes them applicable as references for the FCC-ee and ILC with appropriate luminosity scaling.

This paper presents sensitivity studies on the direct production of staus and smuons, wherein each slepton is assumed to decay into a lepton (τ or μ) and the lightest neutralino ($\tilde{\chi}_1^0$), as illustrated in Fig. 1. In this scenario, the lightest neutralino acts as the LSP and is assumed to be purely Bino in composition.

II. DETECTOR, SOFTWARE, AND SAMPLES

The CEPC Conceptual Design Report (CDR) provides a comprehensive introduction to the detector and associated software [37]. For this Monte Carlo (MC) study, the CEPC baseline detector is employed in full MC simulations, which adhere to the particle flow principle and incorporate an ultra-high-granularity calorimetry system, a low-material silicon tracker, and a 3 Tesla magnetic field. The CEPC baseline tracker comprises a silicon tracking system and barrel time projection chamber (TPC), which results in nearly 100% reconstruction efficiencies for muon tracks and tau-decay tracks. In addition, the momentum resolution of muon tracks reaches the per-mille level for momenta ranging from 10 to 100 GeV in the barrel region.

The software employed in the simulation process is as follows: SM background samples were generated using Whizard 1.95 [38], with the version consistent with that used in the official CEPC MC production. SUSY signal samples were generated using MadGraph 2.7.3 [39] and Pythia8 [40]. Particle interactions with detector materials were simulated via MokkaC [41]. Track reconstruction was performed using MarlinTraking [42]. The particle flow algorithm, Arbor [32], was utilized to reconstruct all final-state particles. Lepton identification was implemented using LICH [43], which is based on multivariate data analysis via TMVA [44].

In this study, sleptons are pair-produced in electron-positron collisions, with each slepton decaying into a lepton and the lightest neutralino ($\tilde{\chi}_1^0$) with a 100% branching ratio. For simplifying the analysis, other supersymmetric particles are excluded from the production or decay chains. The mixing matrices for the scalar tau and muon sectors are considered antidiagonal, precluding mixed production modes. Signal samples for direct stau (smuon) production are parametrized as functions of the masses of $\tilde{\tau}$ ($\tilde{\mu}$) and LSP. The $\tilde{\tau}$ ($\tilde{\mu}$) mass range is con-

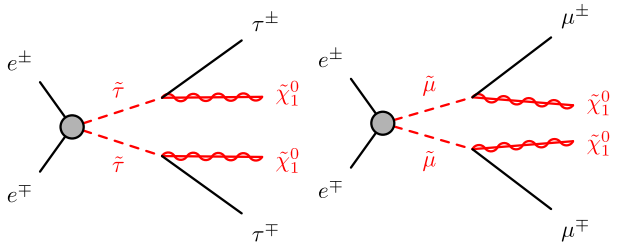

(a) direct stau production (b) direct smuon production

Fig. 1. (color online) Representative diagram illustrating the pair production of charged staus (smuons) and their subsequent decay into a di-tau (di-muon) final state.

strained between the LEP limits [19−24] and CEPC beam energy, spanning 80–179 GeV. Here, left- and right-handed slepton superpartners are assumed to be mass-degenerate. Reference points with $\tilde{\tau}$ ($\tilde{\mu}$) masses of 160 (170) GeV and $\tilde{\chi}_1^0$ masses of 50, 110, and 150 (30, 120, and 160) GeV are used to illustrate key analysis features. Theoretical cross sections for slepton pair production at CEPC-360 GeV are calculated at leading order (LO) using `MadGraph` [39], yielding 42.22 fb for $\tilde{\tau}$ (160 GeV) and 22.34 fb for $\tilde{\mu}$ (170 GeV).

In this analysis, SM background processes include both fully decaying $t\bar{t}$ events and non-$t\bar{t}$ processes featuring two leptons (taus, muons, or electrons) with large recoil mass. The background categories comprise $t\bar{t}$ production, two-fermion processes, four-fermion processes, and selected Higgs processes. The Higgs background is restricted to the $\nu\nu H$ channel, encompassing all possible Higgs decay modes. The two-fermion processes include the $\mu\mu$ and $\tau\tau$ final states, while the four-fermion processes include ZZ, WW, single-Z, single-W, and mixed Z/W production. The two-photon background arises from processes including $ee \to eeee$, $ee \to \mu\mu ee$, and $ee \to \tau\tau ee$. The labels for four-fermion processes in Table 1 are defined solely by the distinct manner in which the four final-state fermions associate with the underlying Z and W boson combinations. All such processes incorporate the full set of contributions, including the s-channel, t-channel, and their interference, as required by the SM. In addition, the processes listed in the table are mutually exclusive, with no overlapping event contributions. The two-photon background were generated using the Feynman diagram calculation (FDC) [45], where the two t-channel photon exchange diagrams provide the leading-order contribution for the beamstrah-lung effect. Therefore, higher-order contributions from beamstrahlung are omitted here, and a more precise investigation can be performed if requried in the future. All simulated samples are normalized to an integrated luminosity of 1.0 ab^{-1}. The cross sections of the considered background processes are summarized in Table 1.

Table 1. Cross-sections of the SM background processes considered at CEPC-360 GeV.

Process	Cross section/fb
ZZ or WW ($\to \mu\mu\nu\nu$)	150.87
$\mu\mu$	2430.34
νZ ($Z \to \mu\mu$)	45.63
ZZ ($\to \mu\mu\nu\nu$)	10.42
WW ($\to \ell\ell\nu\nu$)	281.05
$\tau\tau$	2112.22
ZZ or WW ($\to \tau\tau\nu\nu$)	145.92
ZZ ($\to \tau\tau\nu\nu$)	10.25
νZ ($Z \to \tau\tau$)	16.15
$\nu\nu H$ ($H \to$ anything)	53.62
$t\bar{t}$	610.93
$e\nu W$ ($W \to \mu\nu$)	365.99
$e\nu W$ ($W \to \tau\nu$)	365.52
eeZ ($Z \to \nu\nu$)	35.66
eeZ ($Z \to \nu\nu$) or $e\nu W$ ($W \to e\nu$)	248.41
two-photon	3.96E+8

III. SEARCH FOR DIRECT SLEPTON PRODUCTION

Event reconstruction includes three main components: track reconstruction, particle flow reconstruction, and compound physics object reconstruction. Tracks are reconstructed from detector hits using `Clupatra` [42]. Particle flow reconstruction combines track and calorimeter information to reconstruct individual particle-level objects, which are then used to build compound physics objects such as converted photons, taus, and jets. The identification efficiency for light leptons (electrons and muons) exceeds 99.5% for particles with energies above 2 GeV [43]. For electrons and muons with energies below 1 GeV, particularly those in the barrel edge or barrel-endcap transition regions, the identification efficiency is approximately 90%.

The CEPC exhibits distinct properties, including precise energy-momentum conservation (arising from its clean, symmetric initial state), reduced background noise, and a well-defined center-of-mass frame. Variables associated with invariant mass, lepton/photon momentum and energy, angular distributions, and lepton flavor or charge are effective in this context: they capitalize on the clean initial state and predictable final states of the collider to probe new physics with unparalleled precision. Building on this detailed characterization of lepton collider kinematics, the following variables efficiently discriminate signal events from SM backgrounds:

– $|\Delta\phi(\ell, \text{recoil})|$, the difference of azimuth between one lepton and the recoil system.

– $|\Delta\phi(\ell, \ell)|$, the difference of azimuth between two leptons.

– $\Delta R(\ell, \text{recoil})$, the angular distance between one lepton and the recoil system.[1)]

1) $\Delta R = \sqrt{(\Delta\eta)^2 + (\Delta\phi)^2}$, where η is the pseudorapidity which defined in terms of the polar angle θ by $\eta = -\ln\tan(\theta/2)$ and ϕ is the azimuthal angle.

– $\Delta R(\ell,\ell)$, the angular distance between two leptons.

– E_ℓ, the energy of one lepton.

– P_T, the sum of the transverse momentum of two leptons.

– $M_{\ell\ell}$, the invariant mass of two leptons.

– $M_{\rm recoil}$, the recoil mass of the di-lepton pair, as defined in Eq. (1), where l represents a muon (tau) track originating from smuon (stau) pair production.

$$M_{\rm recoil} = \sqrt{(\sqrt{s} - E_{l_1} - E_{l_2})^2 - |\vec{p}_{l_1} + \vec{p}_{l_2}|^2}\,. \tag{1}$$

To mitigate the effect of potential correlations between variables, the optimization of signal regions relies on an N-dimensional scan over the aforementioned kinematic variables, achieved by applying varying cut values. The cut combination yielding the highest signal sensitivity is selected and further validated by reassessing kinematic distributions within the relevant regions. Ultimately, signal regions are defined using the final selected kinematic criteria. To estimate the sensitivity to the signal, the median significance is employed because it offers a more accurate approximation of the true significance in regions where the number of signal events is non-negligible. This significance, denoted as Z_n, is calculated using the method described in Ref. [46], as shown in Eq. (2).

$$Z_n = \left[2\left((s+b)\ln\left[\frac{(s+b)(b+\sigma_b^2)}{b^2+(s+b)\sigma_b^2}\right] - \frac{b^2}{\sigma_b^2}\ln\left[1+\frac{\sigma_b^2 s}{b(b+\sigma_b^2)}\right]\right)\right]^{1/2}. \tag{2}$$

In the calculation of Z_n, both statistical uncertainty and 5% flat systematic uncertainty are incorporated. This approach is widely adopted in optimization studies for new physics searches across experiments such as ATLAS.

A. Search for direct stau production

For preselection in the search for direct stau production, the following criteria are applied: the two most energetic tracks are required for exactly opposite charges, with each satisfying an energy threshold exceeding 2.5 GeV and an absolute pseudorapidity less than 2.5; this criterion is implemented to suppress the two-photon background. In addition, at least one of these two tracks must originate from a hadronic tau decay. The negatively charged track is identified as a tau lepton, while the positively charged track is identified as an anti-tau lepton. Key kinematic distributions after preselection are presented in Fig. 2, demonstrating strong discrimination power between signal events and SM background processes.

Signal behaviors depend on the mass splitting between $\tilde{\tau}$ and $\tilde{\chi}_1^0$ (ΔM), as shown in Fig. 2. Therefore, three signal regions (SRs) are designed to cover the whole $\tilde{\tau}$-$\tilde{\chi}_1^0$ mass parameter space. SR-ΔM^h encompasses the high-ΔM region, SR-ΔM^m covers the medium-ΔM region, and SR-ΔM^l spans the low-ΔM region. The definitions of these signal regions are summarized in Table 2. An upper cut on the tau energy (E_τ) is applied to suppress $\mu\mu$, Z or W mixing, WW, $e\nu W$, and eeZ processes. A lower cut on the sum of the transverse momentum of two leptons (P_T) is implemented to reduce backgrounds from $\tau\tau$, $\mu\mu$, and νZ processes. Given the signal topology, most signal events exhibit a large recoil mass; thus, a lower cut on the invariant mass of the recoil system ($M_{\rm recoil}$) is used to reject $\tau\tau$ and $e\nu W$ processes, as well as other SM processes lacking significant recoil mass. Upper cuts on the $\tau\tau$ invariant mass ($M_{\tau\tau}$) further suppress $\tau\tau$ and $e\nu W$ backgrounds, whereas a lower cut on $M_{\tau\tau}$ in the SR-ΔM^l region is implemented for reducing the two-photon background. Additional suppression of $\tau\tau$ and $\mu\mu$ processes is achieved via selections on $|\Delta\phi(\tau,\tau)|$ and $|\Delta\phi(\tau,\text{recoil})|$. Selections on $\Delta R(\tau,\tau)$ are employed to further reject $\tau\tau$, ZZ, and single-Z processes. The same signal regions are used for both left-handed and right-handed staus, as their kinematic behaviors are nearly identical, with only small differences in production cross sections.

The kinematic distributions of $M_{\rm recoil}$ and $M_{\tau\tau}$ after applying signal region requirements except those on the variable to be shown are presented in Fig. 3. The lower panel of each plot displays the expected sensitivity Z_n as a function of $M_{\rm recoil}$ and $M_{\tau\tau}$, respectively, demonstrating that the requirements on these variables effectively distinguish signal events from the SM backgrounds. Table 3 summarizes the event yields from background processes and reference signal points after applying the full signal region criteria. The dominant background contributions originate from $ZZ\to\tau\tau\nu\nu$, $\nu Z, Z\to\tau\tau$, ZZ or $WW\to\tau\tau\nu\nu$, $ZZ\to\mu\mu\nu\nu$, $WW\to\ell\ell\nu\nu$, $\nu Z, Z\to\mu\mu$, $\tau\tau$, and $\mu\mu$ processes.

Figure 4 presents the projected exclusion (2σ) and discovery (5σ) contours for direct $\tilde{\tau}$ production, under the assumption of 0% systematic uncertainties (no systematics) and 5% systematic uncertainties. The sensitivity of each signal point is derived using the optimum expected limits from SR-ΔM^h, SR-ΔM^m, and SR-ΔM^l. To assess the effect of detector-related systematics, a conservative 5% flat systematic uncertainty consistent with the LEP experiment is adopted. Under this framework, the discovery reach extends up to 170 GeV for the combined left- and right-handed stau scenario, and up to 169 GeV and 162 GeV for purely left-handed and right-handed staus, respectively. These results indicate only limited de-

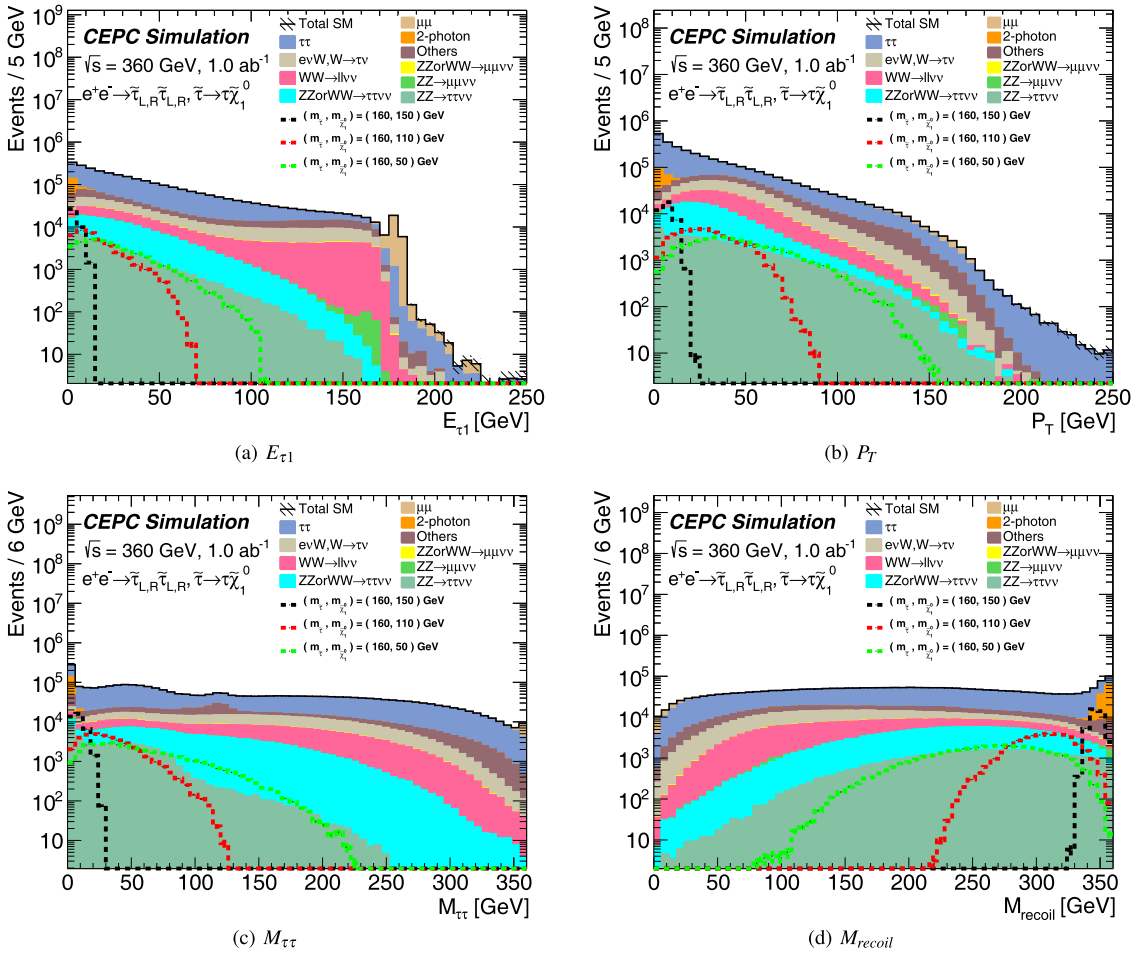

(a) $E_{\tau 1}$ (b) P_T

(c) $M_{\tau\tau}$ (d) M_{recoil}

Fig. 2. (color online) Kinematic distributions for direct stau pair production after the two OS tau selection with E_τ larger than 2.5 GeV. The stacked histograms show the expected SM background. The distributions of three SUSY reference points are shown as dashed lines.

Table 2. Selection requirements for direct stau production signal regions. ΔM represents the mass difference between the $\tilde{\tau}$ and LSP.

SR-ΔM^h	SR-ΔM^m	SR-ΔM^l
E_τ < 40 GeV	E_τ < 15 GeV	
P_T > 50 GeV	P_T > 20 GeV	–
2.55 < $\lvert\Delta\phi(\tau,\text{recoil})\rvert$ < 3.1	$\lvert\Delta\phi(\tau,\text{recoil})\rvert$ < 3.1	2.3<$\lvert\Delta\phi(\tau,\text{recoil})\rvert$ < 2.6
–	0.45< $\Delta R(\tau,\tau)$ < 1.7	$\Delta R(\tau,\tau)$ > 0.45
$\Delta R(\tau,\text{recoil})$ < 3.2	$\Delta R(\tau,\text{recoil})$ < 3.15	$\Delta R(\tau,\text{recoil})$ < 2.8
$M_{\tau\tau}$ < 40 GeV	$M_{\tau\tau}$ < 25 GeV	5 GeV<$M_{\tau\tau}$ < 16 GeV
M_{recoil} > 180 GeV	M_{recoil} > 280 GeV	M_{recoil} > 325 GeV

gradation of sensitivity caused by detector systematics. The most sensitive signal region is selected for each individual point, and therefore, adjacent signal points in overlapping regions may be associated with different signal regions; this can result in non-smooth contours. The resulting limits extend the LEP exclusion bounds by approximately 74 GeV and bridge the gap in the exclusion reach of LHC experiments within the compressed region, as reported in Ref. [30].

B. Search for direct smuon production

For smuon pair production, events that contain exactly two OS muons are selected; each muon satisfies an energy threshold exceeding 2.5 GeV and an absolute pseudorapidity less than 2.5. This criterion is implemented to suppress the two-photon background. The kinemat-

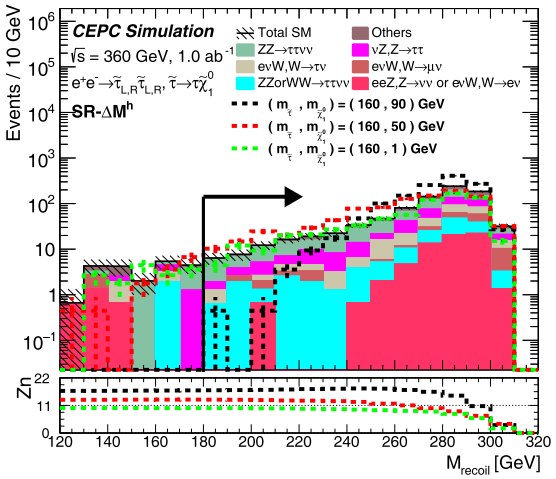

(a) M_{recoil}

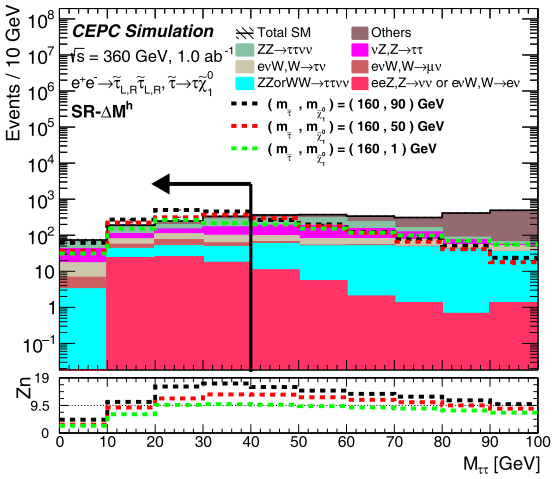

(b) $M_{\tau\tau}$

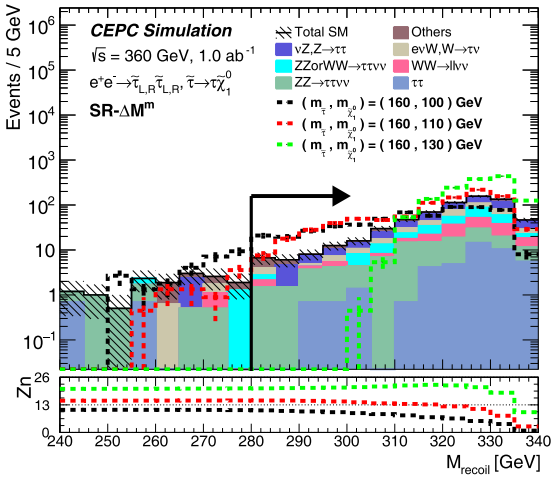

(c) M_{recoil}

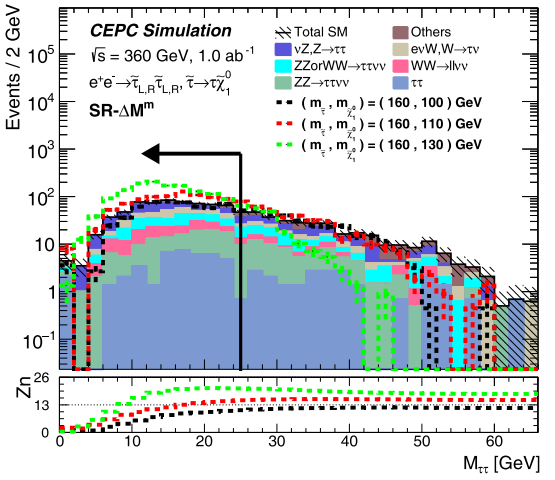

(d) $M_{\tau\tau}$

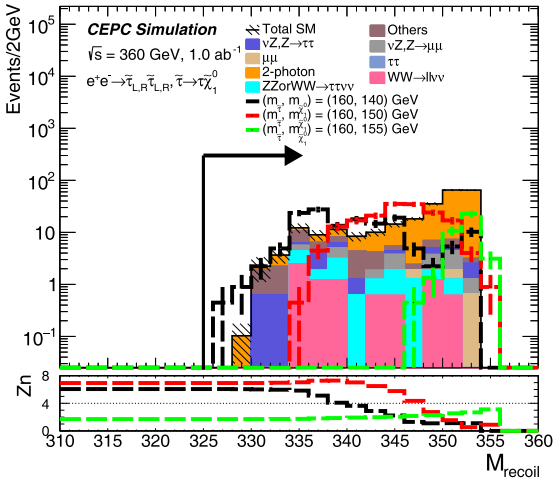

(e) M_{recoil}

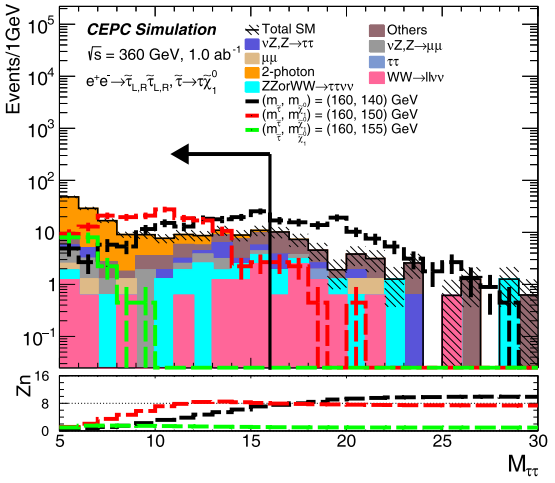

(f) $M_{\tau\tau}$

Fig. 3. (color online) "N-1" distributions after signal region requirements for direct stau pair production. All signal region requirements are applied except for the variable shown. The stacked histograms show the expected SM backgrounds. The distributions from SUSY reference points are shown as dashed lines. The lower pad is the sensitivity Z_n calculated with a statistical uncertainty and a 5% flat systematic uncertainty.

Table 3. Number of events in the signal regions for signal and SM backgrounds with statistical uncertainty for direct stau production.

Process	SR-ΔM^h	SR-ΔM^m	SR-ΔM^l
ZZ or WW ($\to \tau\tau\nu\nu$)	78±7	107±8	8.2±2.3
$\tau\tau$	15±4	52±7	0.0±0.0
νZ ($Z \to \tau\tau$)	161±10	165±10	7.5±2.2
ZZ ($\to \tau\tau\nu\nu$)	239±11	90±7	4.5±1.5
WW ($\to \ell\ell\nu\nu$)	68±7	78±7	4.9±1.7
νZ ($Z \to \mu\mu$)	2.5±1.3	15±4	6.3±2.0
$\mu\mu$	0.0±0.0	5.5±2.0	2.1±1.2
ZZ or WW ($\to \mu\mu\nu\nu$)	3±1	0.59±0.59	0.0±0.0
ZZ ($\to \mu\mu\nu\nu$)	1.3±0.9	0.63±0.63	1.9±1.1
$e\nu W$ ($W \to \tau\nu$)	103±8	100±8	5.0±1.8
$e\nu W$ ($W \to \mu\nu$)	52±6	7.0±2.2	0.0±0.0
eeZ ($Z \to \nu\nu$) or $e\nu W$ ($W \to e\nu$)	62±7	15±3	0.0±0.0
eeZ ($Z \to \nu\nu$)	3.2±1.1	0.0±0.0	0.0±0.0
$\nu\nu H$ ($H \to$ anything)	43±5	17±3	0.7±0.7
2-photon	0.0±0.0	0.0±0.0	105.6±2.3
Total SM	835±22	652±20	146±5
$m(\tilde{\tau},\tilde{\chi}_1^0)$ = (160,50) GeV	946±21	103±7	0.9±0.6
$m(\tilde{\tau},\tilde{\chi}_1^0)$ = (160,110) GeV	958±21	909±20	18±3
$m(\tilde{\tau},\tilde{\chi}_1^0)$ = (160,150) GeV	0.0±0.0	3.1±1.2	151±8

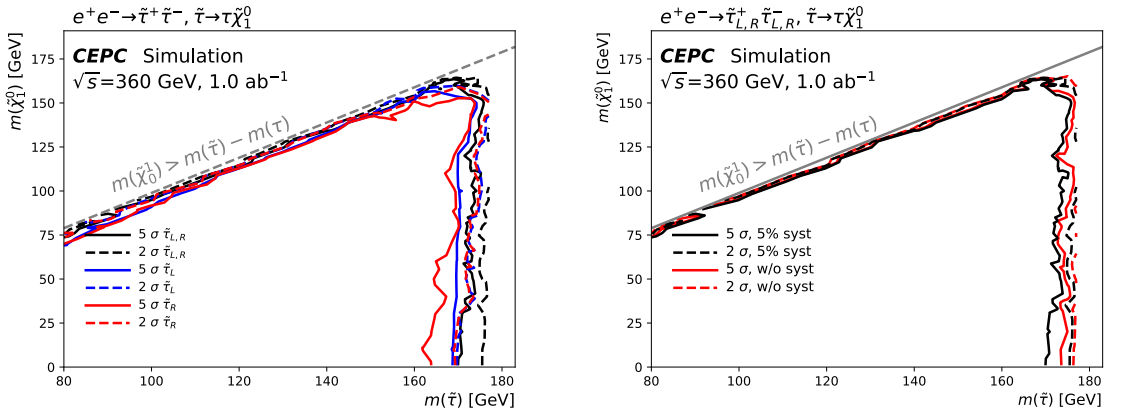

(a) systematic uncertainty = 5% (b) comparison between systematic uncertainty = 0% and 5 %

Fig. 4. (color online) Projected exclusion (2σ) and discovery (5σ) contours for direct $\tilde{\tau}$ production at the CEPC.

ic distributions of the variables used in the analysis, after applying the above selection criteria, are presented in Fig. 5, which demonstrates strong discrimination power between signal events and the SM background processes.

Similar to stau pair production, three SRs are designed to cover different mass splittings between $\tilde{\mu}$ and $\tilde{\chi}_1^0$ (ΔM). SR-ΔM^h encompasses the high-ΔM region, SR-ΔM^m covers the medium-ΔM region, and SR-ΔM^l spans the low-ΔM region. To enhance signal sensitivity, the SR-ΔM^h and SR-ΔM^m regions are further subdivided into intervals based on the energies of the leading and subleading muons ($E_{\mu 1}$ and $E_{\mu 2}$, collectively denoted as $E_{\mu 1,2}$), where $\mu 1$ ($\mu 2$) refers to the muon with the highest (second-highest) energy. The definitions of signal regions are summarized in Table 4 Selections on $E_{\mu 1,2}$ are applied to reject the $\tau\tau$ and νZ background processes. Cuts on $\Delta R(\mu,\text{recoil})$ are used to suppress $\tau\tau$, $\mu\mu$, and ZZ backgrounds, while cuts on the dimuon invariant mass $M_{\mu\mu}$ target the suppression of WW, $\mu\mu$, two-photon and other Z-related backgrounds. Consistent with signal topology, where most signal events exhibit a large recoil mass, a lower cut on the invariant mass of the recoil sys-

Table 4. Selection requirements for direct smuon production signal regions. ΔM represents the mass difference between the $\tilde{\mu}$ and LSP.

SR-ΔM^h	SR-ΔM^m	SR-ΔM^l
$E_{\mu 1,2} > 60$ GeV	$E_{\mu 1,2} < 80$ GeV	$E_{\mu 1,2} > 2.5$ GeV
$E_{\mu 1,2} \in (60-70, >70)$ GeV	$E_{\mu 1,2} \in (<35, 35-80)$ GeV	$\Delta\Phi(\mu, \text{recoil}) < 2.6$
$\Delta R(\mu, \text{recoil}) < 2.8$	$1.9 < \Delta R(\mu, \text{recoil}) < 2.9$	$1.9 < \Delta R(\mu, \text{recoil}) < 2.8$
$M_{\mu\mu} < 87$ GeV $\|\|$ $95 < M_{\mu\mu} < 130$ GeV	$M_{\mu\mu} < 80$ GeV	$M_{\mu\mu} > 5$ GeV
$M_{\text{recoil}} > 100$ GeV	–	$M_{\text{recoil}} > 340$ GeV
$M_{\text{extra}} < 15$ GeV	$M_{\text{extra}} < 10$ GeV	$M_{\text{extra}} < 10$ GeV

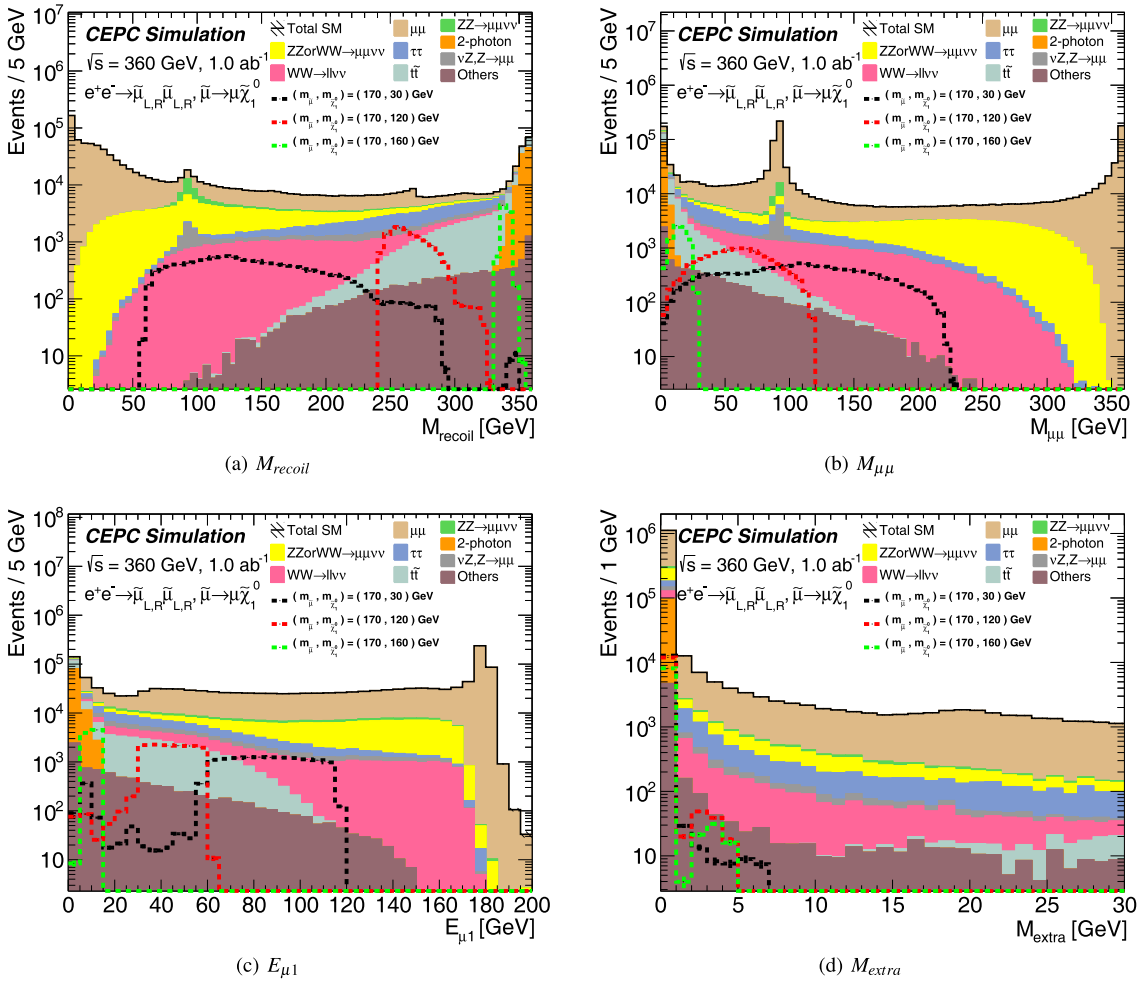

(a) M_{recoil} (b) $M_{\mu\mu}$

(c) $E_{\mu 1}$ (d) M_{extra}

Fig. 5. (color online) Kinematic distributions for direct smuon pair production after applying the preselection. The stacked histograms show the expected SM background. The distributions of three SUSY reference points are shown as dashed lines.

tem (M_{recoil}) is implemented to reject $\mu\mu$, Z, or W mixing processes, and other SM processes lacking significant recoil mass. In addition, the invariant mass of all extra reconstructed visible particles (with energies above 0.5 GeV, excluding two oppositely charged muon tracks), denoted as M_{extra}, is utilized to strongly suppress the $t\bar{t}$ background.

The kinematic distributions of M_{recoil}, $M_{\mu\mu}$, $E_{\mu 1}$, and ΔR (μ, recoil) after applying all signal region requirements except those on the variable being displayed are presented in Fig. 6. The lower panel of each plot shows the expected sensitivity Z_n as a function of M_{recoil}, $M_{\mu\mu}$, $E_{\mu 1}$, and ΔR (μ, recoil), respectively, which demonstrates that selections on M_{recoil} and $M_{\mu\mu}$ effectively distinguish SUSY signal events from the SM background processes. Table 5 summarizes the event yields from all background processes and reference signal points after applying the full signal region criteria. The dominant background con-

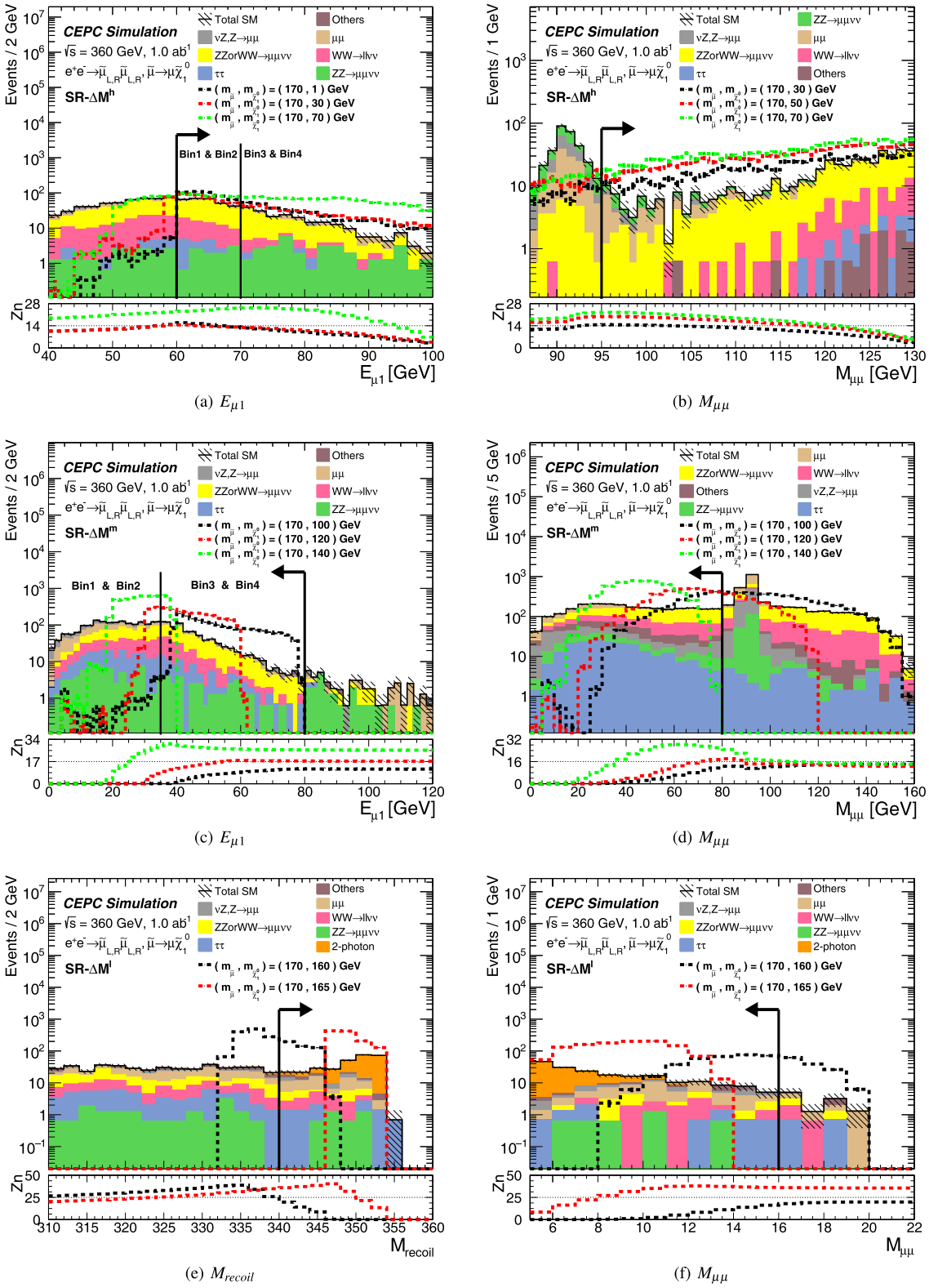

(a) $E_{\mu 1}$ (b) $M_{\mu\mu}$

(c) $E_{\mu 1}$ (d) $M_{\mu\mu}$

(e) M_{recoil} (f) $M_{\mu\mu}$

Fig. 6. (color online) "N-1" distributions after signal region requirements for direct smuon pair production. All signal region requirements are applied except for the variable shown. The stacked histograms show the expected SM backgrounds. The distributions from SUSY reference points are shown as dashed lines. The lower pad is the sensitivity Z_n calculated with a statistical uncertainty and a 5% flat systematic uncertainty.

Table 5. Number of events in the signal regions for signal and SM backgrounds with statistical uncertainty for direct smuon production.

Process	SR-DM^h				SR-DM^m				SR-DM^l
	$E_{\mu1,2} > 60$ GeV				$E_{\mu1,2} < 80$ GeV				
	Bin1	Bin2	Bin3	Bin4	Bin1	Bin2	Bin3	Bin4	
	$60< E_{\mu1} <70$ $60< E_{\mu2} <70$	$60< E_{\mu1} <70$ $E_{\mu2} >70$	$E_{\mu1} >70$ $60< E_{\mu2} <70$	$E_{\mu1} >70$ $E_{\mu2} >70$	$E_{\mu1} <35$ $E_{\mu2} <35$	$E_{\mu1} <35$ $35< E_{\mu2} < 80$	$35< E_{\mu1} < 80$ $E_{\mu2} <35$	$35< E_{\mu1} < 80$ $35< E_{\mu2} < 80$	
ZZ or $WW\,(\rightarrow \tau\tau\nu\nu)$	4.4 ± 1.7	2.5 ± 1.3	0.6 ± 0.6	0.0 ± 0.0	65 ±6	10.0 ± 3.0	16.0 ± 3.0	6.9 ±2.1	2.5 ± 1.3
$\tau\tau$	9.0± 2.5	0.0 ± 0.0	2.1 ± 1.2	0.0 ± 0.0	132 ± 10	21 ± 4	33 ± 5	23 ± 4	2.8 ± 1.4
$\nu Z\,(Z \rightarrow \tau\tau)$	0.0 ± 0.0	0.0 ± 0.0	0.0 ± 0.0	0.0 ± 0.0	54 ± 6	3.8 ± 1.5	5.0 ± 1.8	3.8 ± 1.5	3.8 ± 1.5
$ZZ\,(\rightarrow \tau\tau\nu\nu)$	0.0 ± 0.0	0.5 ± 0.5	0.5 ± 0.5	0.0 ± 0.0	27 ± 4	4.0 ±1.4	5.5 ± 1.7	5.0 ± 1.6	3.0 ± 1.2
$WW\,(\rightarrow \ell\ell\nu\nu)$	39 ± 5	12.0 ± 3.0	11.0 ± 3.0	2.5 ± 1.2	228 ± 12	58 ± 6	97 ± 8	61 ± 6	11.0,2.6
$\nu Z\,(Z \rightarrow \mu\mu)$	3.8 ± 1.5	1.9 ± 1.1	5.6 ± 1.9	8.1 ± 2.3	132 ± 9	18.0 ± 3.0	39 ± 5	16.0 ± 3.0	15.6 ± 3.1
$\mu\mu$	16.0 ± 3.0	12.0 ± 3.0	15.0 ± 3.0	21 ± 4	337 ± 15	31 ± 5	40 ± 5	33 ± 5	36 ± 5
ZZ or $WW\,(\rightarrow \mu\mu\nu\nu)$	112 ± 8	73 ± 7	81 ± 7	46 ± 5	329 ± 14	134 ± 9	271 ± 13	135 ± 9	11.7 ± 2.6
$ZZ\,(\rightarrow \mu\mu\nu\nu)$	1.9 ± 1.1	8.1 ± 2.2	9.4 ± 2.4	24 ± 4	64 ± 6	8.1 ± 2.3	23 ± 4	8.1 ± 2.4	4.4 ± 1.7
$\nu\nu\,H\,(H \rightarrow$ anything)	0.0 ± 0.0	0.8 ± 0.8	0.0 ± 0.0	0.8 ± 0.8	12.0 ± 3.0	5.0 ± 2.0	5.0 ± 2.0	3.3 ± 1.7	0.0 ± 0.0
$t\bar{t}$	0.07 ± 0.07	0.0 ± 0.0	0.0 ± 0.0	0.0 ± 0.0	0.07 ± 0.07	0.0 ± 0.0	0.07 ± 0.07	0.0 ± 0.0	0.0 ± 0.0
2-photon	0.0 ± 0.0	0.0 ± 0.0	0.0 ± 0.0	0.0 ± 0.0	0.0 ± 0.0	0.0 ± 0.0	0.0 ± 0.0	0.0 ± 0.0	106.1 ± 2.3
Total SM	185 ± 11	111 ± 8	125 ± 9	103 ± 8	1379 ± 29	293 ± 13	535 ± 18	294 ± 13	186 ± 7
$m(\tilde{\mu},\tilde{\chi}_1^0) = (170, 30)$ GeV	163 ± 5	200 ± 6	219 ± 6	192 ± 6	8.6 ± 1.2	15.0 ± 2.0	57.0 ± 3.0	0.66 ± 0.33	4.3 ± 0.8
$m(\tilde{\mu},\tilde{\chi}_1^0) = (170,100)$ GeV	453 ± 9	311 ± 7	300 ± 7	46.0 ± 3.0	3.0 ± 0.7	10 ± 1	1870 ± 18	43.0 ± 3.0	1.2 ± 0.4
$m(\tilde{\mu},\tilde{\chi}_1^0) = (170,165)$ GeV	0.0 ± 0.0	0.0 ± 0.0	0.0 ± 0.0	0.0 ± 0.0	2310 ± 20	0.0 ± 0.0	0.0 ± 0.0	0.0 ± 0.0	1158 ± 14

tributions originate from ZZ or $WW \to \mu\mu\nu\nu$, $\mu\mu$, $WW \to \ell\ell\nu\nu$, $ZZ \to \mu\mu\nu\nu$, $\tau\tau$, ZZ or $WW \to \tau\tau\nu\nu$, and $\nu Z(Z \to \tau\tau)$ processes.

Figure 7 shows the projected exclusion (2σ) and discovery (5σ) contours for direct smuon production, assuming 0% and 5% systematic uncertainties. The sensitivity at each signal point is derived using the optimal expected limits from SR-ΔM^h, SR-ΔM^m, and SR-ΔM^l. Under the assumption of a 5% flat systematic uncertainty, the discovery reach extends up to 178 GeV in $\tilde{\mu}$ mass, with minimal degradation attributed to detector-related systematics. The most sensitive signal region is selected for each individual point, and therefore, adjacent signal points in overlapping regions may be associated with different signal regions, potentially resulting in non-smooth contours. This result extends the LEP exclusion limits by approximately 79 GeV and bridges the gap in the compressed mass region left by LHC experiments, as documented in Ref. [30].

C. Summary of slepton search

Figure 8 presents the projected exclusion and discovery contours at the CEPC for direct $\tilde{\tau}$ and $\tilde{\mu}$ production, assuming a 5% flat systematic uncertainty. For direct stau production, the discovery reach extends up to 170 GeV in stau mass for the combined left- and right-handed scenario, with respective reaches of 169 and 162 GeV for purely left-handed and right-handed staus. For direct smuon production, the discovery potential reaches up to 178 GeV in smuon mass. Given the similar design and performance characteristics of future e^+e^- collider facilities, these results serve as a valuable reference for other proposed experiments with comparable center-of-mass energies and target luminosities such as the ILC [34] and FCC-ee [35].

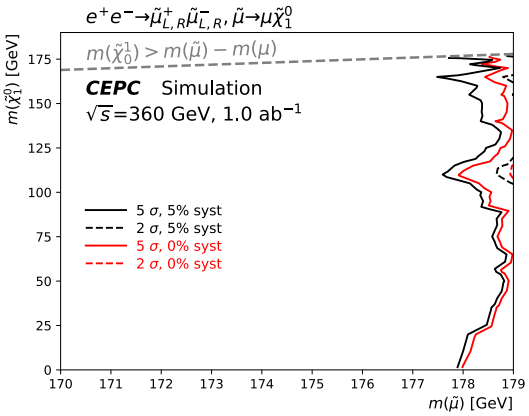

Fig. 7. (color online) Projected exclusion (2σ) and discovery (5σ) contours for direct $\tilde{\mu}$ production at the CEPC, under the assumptions of 0% and 5% systematic uncertainties.

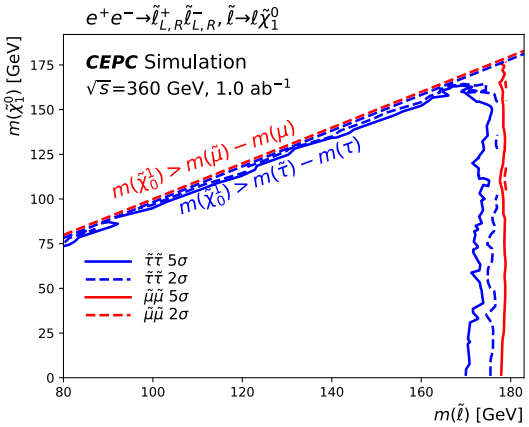

Fig. 8. (color online) Projected exclusion (2σ) and discovery (5σ) contours for direct $\tilde{\tau}$ and direct $\tilde{\mu}$ production at the CEPC, under the assumptions of 5% systematic uncertainties.

IV. CONCLUSION

Searches for direct slepton pair production are performed at the CEPC using fully simulated MC samples, assuming a center-of-mass energy of $\sqrt{s} = 360$ GeV and an integrated luminosity of 1.0 ab^{-1}. The mass reach for $\tilde{\tau}$ ($\tilde{\mu}$) extends approximately 74 (79) GeV beyond the previous limits set by the LEP in the high-mass region. Furthermore, the analysis exhibits sensitivity to the compressed mass region, where the mass difference between $\tilde{\tau}$ ($\tilde{\mu}$) and the LSP is small. This regime remains challenging for ATLAS and CMS to probe effectively. This MC study provides compelling motivation for upgrading the center-of-mass energy of the CEPC from 240 GeV to 360 GeV, enhancing its capability to search for sleptons.

ACKNOWLEDGEMENTS

The authors are grateful to Manqi Ruan, Chengdong Fu, Gang Li, Xianghu Zhao, Ronggang Ping, and Dan Yu for their valuable assistance with CEPC simulations and to Lorenzo Feligioni for helpful input on polishing and improving the manuscript.

References

[1] Y. A. Golfand and E. P. Likhtman, JETP Lett. **13**, 323 (1971)
[2] D. V. Volkov and V. P. Akulov, Phys. Lett. B **46**, 109 (1973)
[3] J. Wess and B. Zumino, Nucl. Phys. B **70**, 39 (1974)
[4] J. Wess and B. Zumino, Nucl. Phys. B **78**, 1 (1974)
[5] S. Ferrara and B. Zumino, Nucl. Phys. B **79**, 413 (1974)
[6] A. Salam and J. A. Strathdee, Phys. Lett. B **51**, 353 (1974)
[7] S. P. Martin, Adv. Ser. Dir. High Energy Phys. **18**, 1 (1998)
[8] G. R. Farrar and P. Fayet, Phys. Lett. B **76**, 575 (1978)

[9] H. Goldberg, Phys. Rev. Lett. **50**, 1419 (1983)
[10] J. R. Ellis, J. S. Hagelin, D. V. Nanopoulos *et al.*, Nucl. Phys. B **238**, 453 (1984)
[11] D. Albornoz Vásquez, G. Bélanger, and C. Bœhm, Phys. Rev. D **84**, 095015 (2011)
[12] G. Belanger, F. Boudjema, A. Cottrant *et al.*, Nucl. Phys. B **706**, 411 (2005)
[13] S. F. King, J. P. Roberts, and D. P. Roy, JHEP **10**, 106 (2007)
[14] M. Dine and W. Fischler, Phys. Lett. B **110**, 227 (1982)
[15] L. Alvarez-Gaume, M. Claudson, and M. B. Wise, Nucl. Phys. B **207**, 96 (1982)
[16] C. R. Nappi and B. A. Ovrut, Phys. Lett. B **113**, 175 (1982)
[17] L. Randall and R. Sundrum, Nucl. Phys. B **557**, 79 (1999)
[18] G. F. Giudice, M. A. Luty, H. Murayama *et al.*, JHEP **12**, 027 (1998)
[19] LEPSUSYWG, ALEPH, DELPHI, L3 and OPAL experiments, note LEPSUSYWG/04-01.1. URL http://lepsusy.web.cern.ch/lepsusy/Welcome.html
[20] A. Heister, S. Schael, R. Barate *et al.*, Physics Letters B **526**, 206 (2002)
[21] A. Heister, S. Schael, R. Barate *et al.*, Phys. Lett. B **583**, 247 (2004)
[22] J. Abdallah *et al.* (DELPHI Collaboration), Eur. Phys. J. C **31**, 421 (2003)
[23] P. Achard, O. Adriani, M. Aguilar-Benitez *et al.*, Phys. Lett. B **580**, 37 (2004)
[24] G. Abbiendi *et al.* (OPAL Collaboration), Eur. Phys. J. C **32**, 453 (2004)
[25] G. Aad *et al.* (ATLAS Collaboration), Eur. Phys. J. C **80**, 123 (2020)
[26] A. Hayrapetyan *et al.* (CMS Collaboration), Phys. Rev. D **109**, 112001 (2024)
[27] G. Aad *et al.* (ATLAS Collaboration), Phys. Rev. D **101**, 052005 (2020)
[28] G. Aad *et al.* (ATLAS Collaboration), JHEP **05**, 150 (2024)
[29] A. M. Sirunyan *et al.* (CMS Collaboration), Eur. Phys. J. C **80**, 189 (2020)
[30] G. Aad *et al.* (ATLAS Collaboration), Phys. Rept. **1116**, 261 (2025)
[31] A. Dainese, M. Mangano, A. B. Meyer *et al.*, *Physics of the HL-LHC, and Perspectives at the HE-LHC. CERN Yellow Reports: Monographs*, CERN-2019-007, CERN (2019)
[32] M. Ruan, H. Zhao, G. Li *et al.*, Eur. Phys. J. C **78**(5), 426 (2018)
[33] J. Yuan *et al.*, (2022), arXiv: 2203.10580
[34] T. Behnke, J. E. Brau, P. N. Burrows *et al.*, (2013), arXiv: 2010.15061
[35] M. Bicer, H. Duran Yildiz, I. Yildiz *et al.*, JHEP **01**, 164 (2014)
[36] I. Smiljanic, I. Bozovic Jelisavcic, and G. Kacarevic, (2020), arXiv: 2010.15061
[37] The CEPC Study Group, (2018), arXiv: 1811.10545
[38] W. Kilian, T. Ohl, and J. Reuter, Eur. Phys. J. C **71**, 1742 (2011)
[39] J. Alwall, R. Frederix, S. Frixione *et al.*, JHEP **07**, 079 (2014)
[40] T. Sjöstrand, S. Ask, J. R. Christiansen *et al.*, Comput. Phys. Commun. **191**, 159 (2015)
[41] P. Mora de Freitas, H. Videau, Detector simulation with MOKKA / GEANT4: Present and future, In *Proceedings of International Workshop on Linear Colliders (LCWS 2002)*, (Korea: Jeju Island, 2002), p. 623-627
[42] F. Gaede, S. Aplin, R. Glattauer *et al.*, J. Phys. Conf. Ser **513**, 022011 (2014)
[43] D. Yu, M. Ruan, V. Boudry, and H. Videau, Eur. Phys. J. C **77**(9), 591 (2017)
[44] A. Hoecker, P. Speckmayer, J. Stelzer *et al.*, (2007), arXiv: physics/0703039
[45] J. X. Wang, Nucl. Instrum. Meth. A **534**, 241 (2004)
[46] G. Cowan, *Discovery sensitivity for a counting experiment with background uncertainty*, http://www.pp.rhul.ac.uk/~cowan/stat/medsig/medsigNote.pdf, (2021)